Electronic Supplementary Material (ESI) for Physical Chemistry Chemical Physics.
This journal is © the Owner Societies 2019

Supplementary Information

Operando Soft X-ray Emission Spectroscopy of Fe_2O_3 Anode to Observe the Conversion Reaction

Daisuke Asakura[1,2], Yusuke Nanba[1#], Hideharu Niwa[3,4†], Hisao Kiuchi[5‡], Jun Miyawaki[3,4], Masashi Okubo[1$], Masaharu Oshima[4], Eiji Hosono[1,2*], and Yoshihisa Harada[2,3,4].*

[1]Research Institute for Energy Conservation, National Institute of Advanced Industrial Science and Technology (AIST), Tsukuba, Ibaraki 305-8568, Japan

[2]AIST-UTokyo Advanced Operando-Measurement Technology Open Innovation Laboratory (Operando OIL), National Institute of Advanced Industrial Science and Technology (AIST), Kashiwa, Chiba 277-8565, Japan

[3]Institute for Solid State Physics, The University of Tokyo, Kashiwa, Chiba 277-8581, Japan

[4]Synchrotron Radiation Research Organization, The University of Tokyo, Bunkyo-ku, Tokyo 113-8656, Japan

[5]Department of Applied Chemistry, School of Engineering, The University of Tokyo, Bunkyo-ku, Tokyo 113-8656, Japan

AUTHOR INFORMATION

Corresponding Authors

*Daisuke Asakura: daisuke-asakura@aist.go.jp

Research Institute for Energy Conservation, National Institute of Advanced Industrial Science and Technology, 1-1-1 Umezono, Tsukuba Ibaraki 305-8568 JAPAN.

*Eiji Hosono: e-hosono@aist.go.jp

Research Institute for Energy Conservation, National Institute of Advanced Industrial Science and Technology, 1-1-1 Umezono, Tsukuba Ibaraki 305-8568 JAPAN.

Present Addresses

[#]Yusuke Nanba, Center for Green Research on Energy and Environment Materials, National Institute for Materials Science, Tsukuba, Ibaraki 305-0044, Japan

† Hideharu Niwa, Faculty of Pure and Applied Sciences, University of Tsukuba, Tsukuba, Ibaraki 305-8571, Japan

‡ Hisao Kiuchi, Office of Society-Academia Collaboration for Innovation, Uji, Kyoto University, Kyoto 611-0011, Japan

$ Masashi Okubo, Department of Chemical System Engineering, School of Engineering, The University of Tokyo, Bunkyo-ku, Tokyo 113-8656, Japan

Comparison between soft X-ray and hard X-ray spectroscopy and importance of *operando* soft X-ray spectroscopy

X-ray absorption near edge structure (XANES) at the TM *K*-edges ($1s \rightarrow np$ absorption is dominant; $n \geqq 4$) can reveal the oxidation state of the TMs, and extended X-ray absorption fine structure (EXAFS) at the TM *K*-edges gives us information of the local structure around the TM. TM *K*-edges are included in the hard X-ray (HX) region higher than ~5 keV. HX experiments do not need a vacuum condition around the sample, which is favorable for *in situ/operando* analyses of LIB electrodes with liquid electrolytes.[S1] Moreover, the deep probing depth of HX spectroscopies except for hard X-ray photoemission spectroscopy is also suitable for obtaining the information of bulk electronic structures in electrode materials.

However, HX absorption spectroscopies at the TM *K* edges are not so suitable to derive detailed information of the *d* orbitals of TMs due to the dipole selection rule in which $1s \rightarrow np$ absorption is allowed.[S2] For $3d$ TMs, soft X-ray absorption spectroscopy (XAS) is a very powerful method to clarify the $3d$ orbitals. Indeed, many XAS studies at the $3d$ TMs' $L_{2,3}$ edges ($2p_{1/2,3/2} \rightarrow 3d$ absorption) have clarified not only the oxidation states of $3d$ TMs, but also the detailed electronic structures such as the crystal-field splitting, Coulomb interactions among the *d* electrons, charge-transfer (CT) effects with the ligands, and so on.[S2,S3] Soft X-ray (SX) spectroscopies are also beneficial to directly obtain the information of $2p$ orbitals of ligands, e.g. oxygen, because SXs cover the light-elements *K* edges ($1s \rightarrow 2p$ absorption). On the other hand, in general, SX spectroscopies need a vacuum condition, which is disadvantageous for *in situ/operando* electronic-structure analyses of LIB electrodes. Although the redox reactions and electronic-structure changes during the charge-discharge various electrode materials can be revealed in detail by *ex situ* SX spectroscopy depending on the electrode material,[S4-S6] *operando* SX spectroscopy with applying a voltage to the electrodes as with HX experiments is highly demanded particularly for anode materials, because the redox potentials of them in low voltages like < 1 V vs. Li/Li^+ cannot be maintained even for *in situ* conditions without dissembling a battery cell. In order to accurately observe the electronic-structure change during charge-discharge, *operando* SX spectroscopy under a potentiostatic operation is inevitable.

We have developed *operando* soft X-ray emission spectroscopy (XES) by modifying *in situ* techniques for SX spectroscopy of liquid samples,[S7] and we demonstrated the Mn 3*d* electronic-structure analysis on $LiMn_2O_4$ thin-film cathode.[S8] XES is the secondary optical process of XAS: a spectroscopy of the emitted photons when valence electrons fall into the core holes created by the XAS process.[S2,S9,S10] For example, the 3*d* orbitals of TMs can be investigated in detail by the 2*p*-3*d*-2*p* resonant XES. XES has a potential of state-selectivity by tuning the incident photon energy (excitation energy, E_{in}) while XAS spectrum shows overlapping information in case that some states (oxidation states, spin states, etc.) coexist for a specific element in a sample.[S11] For the electrode materials of LIBs, the possible state selectivity of XES is promising to separately clarify the mixed oxidation states during the charge-discharge.

Synchrotron XRD for the Fe_2O_3 thin film

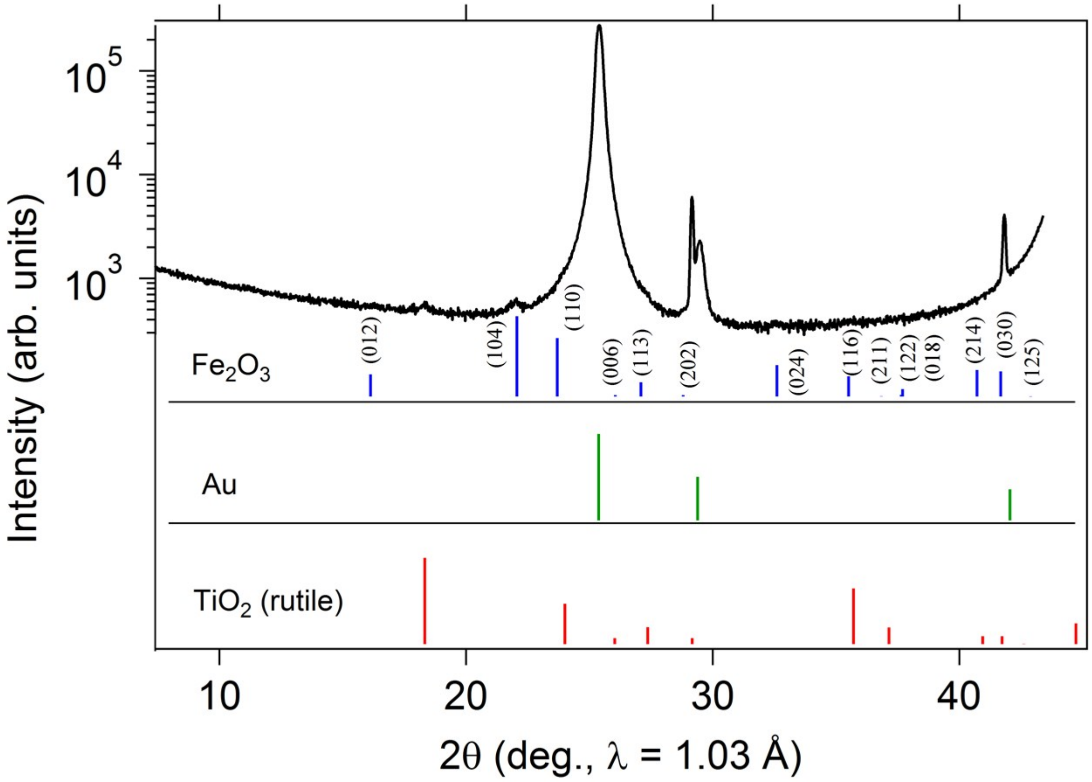

Fig. S1. Synchrotron XRD pattern of the Fe_2O_3 thin film fabricated on the electrode chip (corresponding to the initial state). The wavelength of X-ray λ was set to 1.03 Å. Diffraction patterns of α-Fe_2O_3, Au, and TiO_2 (rutile phase) are also displayed [S12,S13].

Comparison of the CV curves

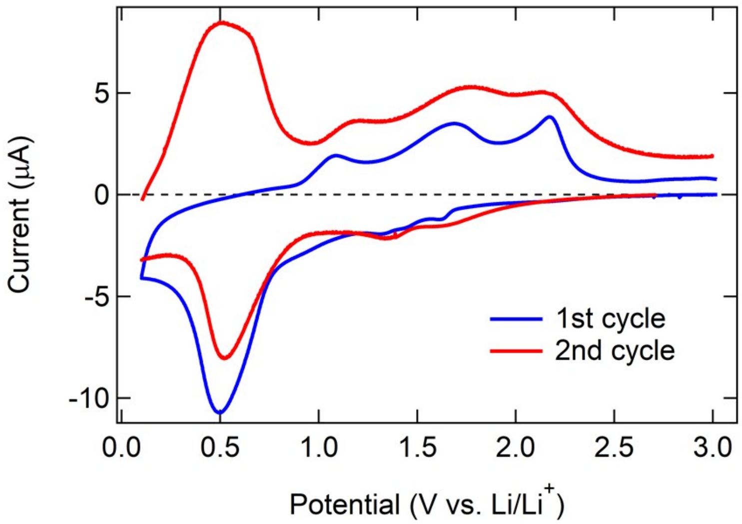

Fig. S2. Comparison of the CV curves between the first and second cycles.

Fe $L_{2,3}$-edge XAS for the as-fabricated Fe_2O_3 thin film

We measured the Fe $L_{2,3}$-edge XAS for the as-fabricated Fe_2O_3 thin film with the partial-fluorescence yield (PFY) mode to determine the excitation energy for XES. As Fig. S3 shows, the Fe L_3-edge has characteristic two peaks labeled as E_{I} and E_{II}, and the L_2-edge has a doublet structure and a shoulder structure around 724.7 eV. CIFM calculation for Fe^{3+} reproduced these peaks. The electronic-structure parameters for the Fe^{3+} state listed in Table S1 are commonly used for the calculation for the XES spectrum in Fig. S4.

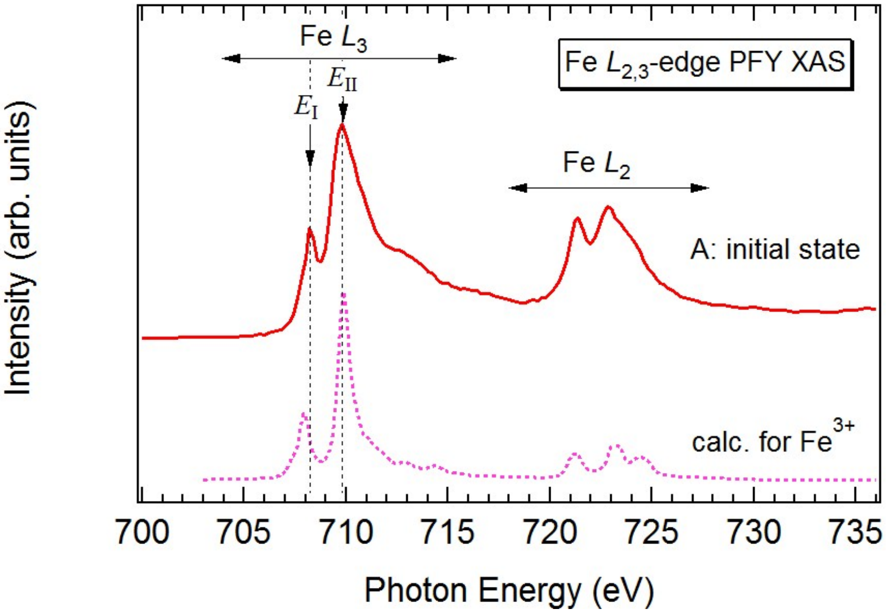

Fig. S3. Fe $L_{2,3}$-edge PFY XAS for the as-fabricated Fe_2O_3 thin film and CIFM calculation for Fe^{3+} state.

Fe 2*p* XES for the as-fabricated thin film with E_{in} = 709.8 eV

For the as fabricated thin film, we also performed Fe 2*p* XES with E_{in} = 709.8 eV corresponding to the Fe L_3 main peak in the XAS spectrum. As Fig. S4 shows, the XES spectrum is similar to the that for single-crystalline Fe_2O_3 by Miyawaki *et al.* [S14] as with the XES result with E_{in} = 708.2 eV. Figure S4 also displays the CIFM calculation for Fe^{3+} state. The electronic-structure parameters are summarized in Table S1. Although the peaks in the calculation are slightly shift, the features of *dd* excitation (0.8 eV < E_{loss} < ~4.0 eV for spectrum for as-fabricated thin film) and CT excitation (E_{loss} > ~4.0 eV for spectrum for as-fabricated thin film) are reproduced. Thus, the as-fabricated thin film has almost the same Fe 3*d* state as that for single-crystalline Fe_2O_3, which are attributed to the Fe^{3+} state.

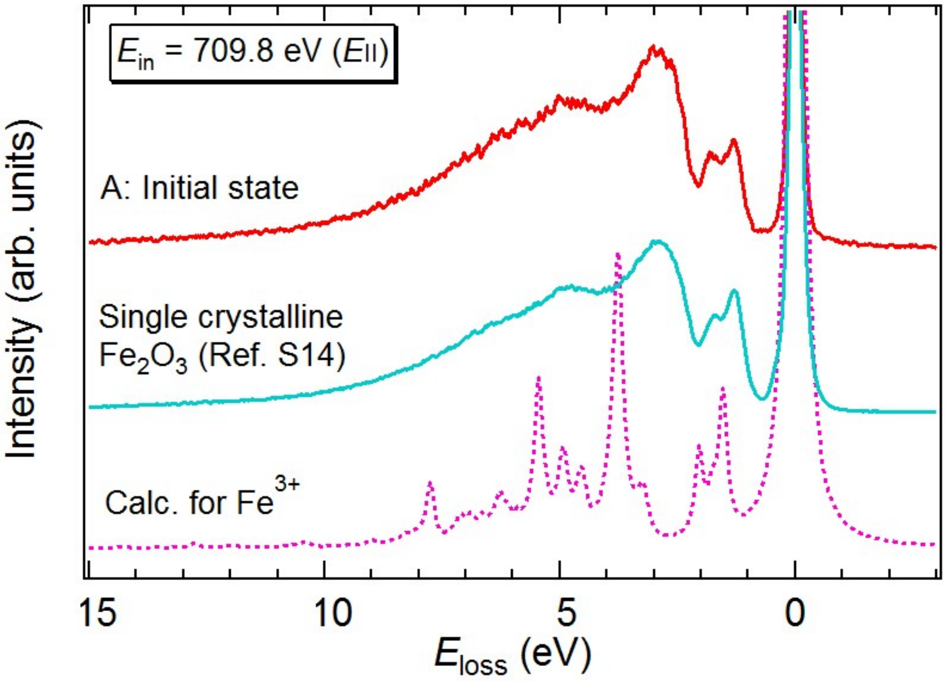

Fig. S4. *Ex situ* Fe 2*p* XES spectra for the as-fabricated thin film and single-crystalline Fe_2O_3 by Miyawaki *et al*. [S14] measured with excitation energy E_{II}. CIFM calculation for Fe^{3+} state is also displayed.

CIFM calculation for the Fe^{3+}, Fe^{2+} and Fe^0 states

For the CIFM calculation of the Fe $L_{2,3}$-edge XAS and Fe 2*p*-3*d*-2*p* RXES in Fe_2O_3, we employed the octahedral $[FeO_6]^{y-}$ (y = 9, 10) cluster with the Hamiltonian as,

$$H = H_{Fe} + \sum_{j,\gamma,\sigma} \varepsilon_P(j\gamma) n_{P,j\gamma\sigma} + \sum_{j,\gamma,\sigma} V_{pd}(j\gamma)\left(d_{\gamma\sigma}^{\dagger} P_{j\gamma\sigma} + h.c.\right), \quad (S1)$$

where $P_{j\gamma\sigma}^{\dagger}$ and $n_{P,j\gamma\sigma}$ represent the electron creation and number operators for O 2*p*, respectively. While the symmetry γ is e_g or t_{2g} irreducible representation, spin σ is ↑ or ↓. The second and third terms in eq. (S1) are the O 2*p* states and Fe 3*d*-O 2*p* hybridization, respectively. These terms are not effective in an atomic calculation (Fe^0). The H_{Fe} is given by

$$H_{Fe} = \sum_{\gamma,\sigma}\left[\varepsilon_d(\gamma) - Q\sum_{m,\sigma}{}^{'}\left(1 - n_{p,m\sigma}{}^{'}\right)\right]n_{d,\gamma\sigma} + \sum_{m,\sigma}\varepsilon_{p,m\sigma}n_{p,m\sigma} + U\sum_{\gamma}n_{d,\gamma\uparrow}n_{d,\gamma\downarrow} + + H_{multi}\ (S2)$$

where $d^{\dagger}_{\gamma\sigma}$, $n_{d,\gamma\sigma}$, and $n_{p,m\sigma}$ represent the Fe 3*d* electron creation operator and the number operators for Fe 3*d* and Fe 2*p*, respectively. *m* represents the magnetic quantum number. The first term in eq. (S2) is the Fe 3*d* states with $\varepsilon_d(\gamma)$ being the one-electron energy level and *Q* being the averaged Coulomb attraction caused by Fe 2*p* core hole. The second term represents the Fe 2*p* states. The third and fourth terms describe the Coulomb and exchange interactions between Fe 3*d* electrons. The last term includes the multipole part of the Fe 3*d*- Fe 3*d* and Fe 3*d*- Fe 2*p* Coulomb interactions that are not described in the third and fourth terms and the spin-orbit interactions for the Fe 3*d* and Fe 2*p* orbitals. The Slater integrals were evaluated using Cowan's code [S15]. In this study, the values were reduced to 85%. For Fe^0 calculation, a term to describe Fe 4*s* electrons, $\sum_{\sigma}\varepsilon_s n_{s,\sigma}$ was considered in the atomic calculation, where $n_{s,\sigma}$ represents the number operator for Fe 4*s*.

In the numerical calculation, the wave function was obtained by the Lanczos method [S16]. The XAS spectrum was calculated using the Fermi's golden rule expressed as,

$$I_{XAS}(\omega_{in}) = \sum_{m}\left|\langle m \left| T_\mu \right| g\rangle\right|^2\delta(\omega_{in} - E_m + E_g),\ (S3)$$

where |*g*> and |*m*> represent the ground (initial) and final state of XAS, respectively, and the corresponding energies are E_g and E_m. The XAS finale state corresponds with the XES intermediate one. When ω_{in} and ω_{out} are the incident and emitted photon energy, the XES spectrum [S17] was expressed as:

$$I_{XES}(\omega_{in},\omega_{out}) = \sum_f \left| \sum_m \frac{\langle f|T_\nu|m\rangle\langle m|T_\mu|g\rangle}{E_g + \omega_{in} - E_m - i\Gamma} \right|^2 \delta(\omega_{out} + E_f - \omega_{in} - E_g). \quad (S4)$$

The final state was denoted as $|f\rangle$ with the energy E_f. T represents the electric dipole operator. The core-hole lifetime broadening effect in the intermediate state (= XAS final state) is taken into account with a constant parameter Γ for Fe 2*p* core-hole level. The theoretical line spectra thus obtained were convoluted, using Lorentzian and Gaussian functions (with each width of 0.6 eV).

The diagonal elements and CT energies used in this study are defined. In the octahedral $[FeO_6]^{9-}$ cluster, the CT energy from high-spin d^5 ($t_{2g}{}^3e_g{}^2$) to $d^6\underline{L}(t_{2g})$ is given as

$$E[d^6\underline{L}] - E[d^5] = \Delta(Fe^{3+}) - 4Dq - \varepsilon_P(t_{2g}), \quad (S5)$$

where $\varepsilon_P(t_{2g})$ is the O 2*p* state hybridized with $3d(t_{2g})$ orbitals. This value is −1.25 eV from the transfer integral value (*pp*σ). The energy of d^5 electron configuration is

$$E[d^5] = 5\varepsilon_d + 10U - 30J + E_0 \qquad (S6)$$

and

$$\Delta(Fe^{3+}) = \varepsilon_d + 5U - 8J. \qquad (S7)$$

The relation between U and the averaged Coulomb interaction $\bar{U}$ is expressed as

$$U = \bar{U} + 4F_2 + 36F_4 \qquad (S8)$$

where F_2 and F_4 are the Slater integrals. In Eq. (S6), E_0 is the sum of the energies of Fe 2*p* electrons and those of ligand electrons. An one-electron energy ε_d is expressed as

$$\varepsilon_d = \frac{2\varepsilon_d(e_g) + 3\varepsilon_d(t_{2g})}{5}. \qquad (S9)$$

The octahedral crystal field splitting is $10Dq = \varepsilon_d(e_g) - \varepsilon_d(t_{2g})$. We also show the averaged CT energy Δ' ($= \varepsilon_d + 5\bar{U}$, for Fe^{3+}) in Table S1 for comparisons with previous studies.

In the tetragonal $[FeO_6]^{10-}$ cluster, the CT energy from high-spin d^6 ($t_{2g}^4 e_g^2$) to $d^7\underline{L}(t_{2g})$ is given as

$$E[d^7\underline{L}] - E[d^6] = \Delta(Fe^{2+}) - 4Dq - \varepsilon_P(t_{2g}). \quad (S10)$$

The energy of d^4 electron configuration is

$$E[d^6] = 6\varepsilon_d + 15U - 38J - 8Dq + E_0 \quad (S11)$$

and

$$\Delta(Fe^{2+}) = \varepsilon_d + 6U - 11J. \quad (S12)$$

The averaged CT energy Δ' ($= \varepsilon_d + 6\bar{U}$, for Fe^{2+}) is also shown in Table S1.

Table S1. Electronic-structure parameters for the Fe^{3+}, Fe^{2+}, and Fe^0 states used in the CIFM calculation (in eV).

	Fe^{3+}	Fe^{2+}	Fe^0
Δ	4.6	3.2	—
Δ’	2.0	1.4	—
U	6.4	6.2	1.7
$\bar{U}$	4.5	4.5	0.0
J	0.9	0.8	0.8
$10Dq$	1.5	0.4	0.0
$(pd\sigma)$	-0.8	-0.6	—

REFERENCES

(S1) B.-M. Chae, E.-S. Oh, and Y.-K. Lee, *J. Power Sources,* 2015, **274**, 748.

(S2) F. M. F. de Groot and A. Kotani, *Core Level Spectroscopy of Solids* (Advances in Condensed Matter Science); CRC Press Taylor & Francis Group: Boca Raton, FL, 2008.

(S3) F. M. F. de Groot, *J. Electron Spectrosc. Relat. Phenom.,* 1994, **67**, 529.

(S4) D. Asakura, M. Okubo, Y. Mizuno, T. Kudo, H. S. Zhou, K. Amemiya, F. M. F. de Groot, J.-L. Chen, W.-C. Wang, P.-A. Glans, C. L. Chang, J.-H. Guo and I. Honma, *Phys. Rev. B,* 2011, **84**, 045117.

(S5) Y. Nanba, D. Asakura, M. Okubo, Y. Mizuno, T. Kudo, H. S. Zhou, K. Amemiya, J.-H. Guo, K. Okada, *J. Phys. Chem. C,* 2012, **116**, 24896.

(S6) for example, (a) S. Kurosumi, K. Horiba, N. Nagamura, S. Toyoda, H. Kumigashira, M. Oshima, S. Furutsuki, S.-i. Nishimura, A. Yamada, and N. Mizuno, *J. Power Sources,* 2013, **226**, 42. (b) L. F. J. Piper, N. F. Quackenbush, S. Sallis, D. O. Scanlon, G. W. Watson, K.-W. Nam, X.-Q. Yang, K. E. Smith, F. Omenya, N. A. Chernova, and M. S. Whittingham, *J. Phys. Chem. C* 2013, **117,** 10383. (c) R. M. Qiao, L. A. Wray, J.-H. Kim, P. W. Pieczonka, S. J. Harris, and W. L. Yang, *J. Phys. Chem. C,* 2015, **119,** 27228. (d) W.-S. Yoon, K.-B. Kim, M.-G. Kim, M.-K. Lee, H.-J. Shin, J.-M. Lee, J.-S. Lee, and C.-H. Yo, *J. Phys. Chem. B,* 2002, **106**, 2526. (e) W.-S. Yoon, K.-Y. Chung, K.-H. Oh, and K.-B. Kim, *J. Power Sources,* 2003, **119-121**, 706.

(S7) H. Niwa, H. Kiuchi, J. Miyawaki, Y. Harada, M. Oshima, Y. Nabae, and T. Aoki, *Electrochem. Commun.,* 2013, **35**, 57.

(S8) D. Asakura, E. Hosono, H. Niwa, H. Kiuchi, J. Miyawaki, Y. Nanba, M. Okubo, H. Matsuda, H. S. Zhou, M. Oshima, and Y. Harada, *Electrochem. Commun.,* 2015, **50**, 93.

(S9) A. Kotani and S. Shin, *Rev. Mod. Phys.,* 2001, **73**, 203.

(S10) L. J. P. Ament, M. van Veenendaal, T. P. Devereaux, J. P. Hill, and J. van den Brink, *Rev. Mod. Phys.,* 2011, **83**, 705.

(S11) D. Asakura, Y. Nanba, M. Okubo, Y. Mizuno, H. Niwa, M. Oshima, H. S. Zhou, K. Okada, K. and Y. Harada, *J. Phys. Chem. Lett.,* 2014, **5**, 4008.

(S12) R. L. Blake, R. E. Hessevick, T. Zoltai, L. W. Finger, *Am. Miner.,* 1966, **51**, 123.

(S13) R. W. G. Wyckoff, *Crystal Structures* (Second Ed., Vol. 1); Interscience Publishers: New York, NY, 1963.

(S14) J. Miyawaki, S. Suga, H. Fujiwara, M. Urasaki, H. Ikeno, H. Niwa, H. Kiuchi, and Y. Harada, *Phys. Rev. B,* 2017, **96**, 214420.

(S15) R. D. Cowan, *The Theory of Atomic Structure and Spectra*; University of California Press: Berkeley, CA, 1981.

(S16) V. Heine, *Solid State Physics*; H. Ehrenreich, F. Seitz, D. Turnbull, Eds.; Academic Press: New York, 1980; Vol. 35, p 87.